Commun. Comput. Phys.
doi: 10.4208/cicp.OA-2017-0100

Vol. **23**, No. 5, pp. 1534-1548
May 2018

Numerical Study of the Isotropic-Nematic Phase Transition in Liquid Crystals using the String Method

Yunzhi Li[1] and Weiqing Ren[1,2,*]

[1] *Department of Mathematics, National University of Singapore, Singapore 119076.*
[2] *Institute of High Performance Computing, Agency for Science, Technology and Research, Singapore 138632.*

Received 3 May 2017; Accepted (in revised version) 10 July 2017

Abstract. We consider a system of liquid crystal modeled by hard spherocylinders. In certain range of the pressure, the system exhibits two metastable phases: the isotropic phase and the nematic phase. In the isotropic phase, the spherocylinders are randomly packed. In contrast, the spherocylinders are well-ordered in the nematic phase. The isotropic-nematic phase transition is a rare event because it involves the crossing of energy barrier(s). This makes direct simulations, e.g. using molecular dynamics, of the transition event infeasible. In this paper, we study the phase transition in a coarse-grained space formed by two collective variables: the order parameter of the spherocylinders and the volume of the system. We compute the free energy in the collective variable space, the minimum free energy path (MFEP) between the isotropic phase and the nematic phase, and the transition state. Our results reveal the multilayer structure of the critical nucleus. The nucleus will grow further and evolve to the nematic phase after it crosses the energy barrier.

AMS subject classifications: 65Z05, 70E55, 82D25

Key words: Phase transition, liquid crystal, order parameter, collective variables, string method.

1 Introduction

Liquid crystals formed by hard rod-like particles exhibit different metastable phases as observed in the experiments [1, 2], including the disordered isotropic phase and the aligned nematic phase. A phase diagram in the space of the concentration and the aspect ratio of the rod-like particles was constructed in Ref. [1]. In certain range of the concentration and the aspect ratio, the isotropic phase and the nematic phase coexist as metastable phases. The isotropic-nematic phase transition is a rare event since it involves the crossing of energy barrier(s). The formation of critical nucleus during the phase transition was

*Corresponding author. *Email addresses:* a0000571@u.nus.edu (Y. Li), matrw@nus.edu.sg (W. Ren)

investigated using computer simulations, such as biased Monte Carlo simulations [3–5]. In this work, we study the mechanism of isotropic-nematic phase transition using the string method [6–11].

A theoretical explanation for the formation of the nematic liquid crystal from the isotropic phase was provided by Onsager [12]. He explained that the isotropic-nematic phase transition could be purely entropy based. Two types of entropies compete here: the orientational entropy drives the system towards the isotropic phase in which both centers and orientations of the particles are randomly distributed, while the translational entropy drives the system towards the ordered nematic phase to minimize the excluded volume. Therefore, the ordering of the rod-like particles is closely related to the entropy of the system. This ordering can be described by an orientational order parameter [13], which measures the average alignment of the particles with respect to a common direction. In this work, we use this order parameter to distinguish the isotropic phase from the nematic phase.

Computer simulations of the particle system using hard spherocylinders play an important role in the current understanding of the liquid crystals. A mathematical model was proposed by Few & Rigby [14] and Vieillard [15], in which the rod-like particles were modeled as hard spherocylinders with radius R and a cylindrical segment of length h. The study of the system using molecular dynamics (MD) simulations was then conducted by Rebertus & Sando [16]. Afterwards, the phase diagram of the spherocylinder system in the space of concentration and aspect ratio h/R of spherocylinders was investigated [17, 18] using the MD simulations. It was shown that in certain range of concentration and aspect ratio, the isotropic phase and the nematic phase may coexist as metastable phases. The isotropic-nematic phase transition was studied using the biased Monte Carlo simulations [3–5]. These studies revealed a lamellar crystallite structure at the early stage of the nucleation. However, the subsequent thickening of the lamella is hindered by the fact that the top and bottom surfaces of the crystallite are preferentially covered by spherocylinders that align parallel to the surface. The energy barrier is too large for the simultaneous formation of multilayer nematic cluster. The lamellar crystallite can only grow laterally, leading to a single layer of nematic phase.

In this work, we use the orientational order parameter and the volume of the system as the collective variables (CVs) and study the isotropic-nematic phase transition in the CVs space. We compute the critical nucleus, the free energy barrier and the minimum free energy path (MFEP) using the string method. We identify the transition state in the CVs space. The atomistic configurations sampled from the transition state exhibit multilayer structures. This approach is similar to the study conducted by Yu *et al*. [19]. In that work, they studied the crystal polymorphism in a particle system. The Steinhardt order parameters were used to distinguish the different metastable phases such as fcc and bcc structures. The order parameters were then selected as the CVs and the mechanism of the phase transition was studied using the string method. For the recent development of the numerical methods in the study of nucleation in phase transformations, we refer to a recent review paper [20].

The paper is organized as follows. In Section 2, we describe the MD system in which the particles are modeled as spherocylinders. In Section 3, we describe the numerical method and present the numerical results for the free energy, the pathway for the isotropic-nematic phase transition, and the transition state. The paper is concluded in Section 4.

2 Mathematical model

We consider a particle system consisting of N hard spherocylinders. Each spherocylinder consists of a cylinder part of length h and a cap in the shape of a hemisphere of radius R at each end. The spherocylinder is characterized by the center $\mathbf{c}$ and the axis of symmetry $\mathbf{u}$ with $\|\mathbf{u}\|=1$. The free motion of the spherocylinder is of two kinds: the translational motion of the center $\mathbf{c}$ and the rotational motion of the symmetry axis $\mathbf{u}$. The rotational motion can be decomposed into two parts: one is the rotation of the spherocylinder about the symmetry axis $\mathbf{u}$ and the other is the rotation of the symmetry axis. Here we neglect the rotational motion of the spherocylinder about the symmetry axis, and only consider the rotational motion of the symmetry axis. We denote the angular momentum by $\boldsymbol{\omega}$. The corresponding mass moment of inertia is given by

$$I=\pi\rho R^5\left[\frac{h}{12R}\left(3+\frac{h^2}{R^2}\right)+\left(\frac{8}{15}+\frac{h^2}{3R^2}+\frac{h}{2R}\right)\right], \tag{2.1}$$

where ρ is the density of the spherocylinder. A derivation of the above mass moment is given in Appendix A. In this work, we assume that each spherocylinder has mass 1. Let V_{sc} be the volume of the spherocylinder, then $\rho=\frac{1}{V_{sc}}$.

The free motion of the spherocylinder is governed by the following ordinary differential equations

$$\begin{aligned}&\dot{\mathbf{c}}=\mathbf{p},\\&I\dot{\mathbf{u}}=\boldsymbol{\omega}\times\mathbf{u},\end{aligned} \tag{2.2}$$

where the dots denote the derivative with respect to time. In Eq. (2.2), the center of the spherocylinder $\mathbf{c}$ is advected by the translational velocity $\mathbf{p}$, and the symmetry axis $\mathbf{u}$ rotates with the angular momentum $\boldsymbol{\omega}$.

The spherocylinders interact with each other only through collision, which is modeled by the pair-wise potential

$$U(d)=\begin{cases}0, & \text{if } d>0,\\ \infty, & \text{if } d=0,\end{cases} \tag{2.3}$$

where d is the surface-to-surface distance between two spherocylinders. When two spherocylinders collide, they will repel each other and move in the opposite directions. Fig. 1 shows the situation when two spherocylinders i and j are in contact. Denote by $\mathbf{r}_i$ and $\mathbf{r}_j$ the vectors from the centers $\mathbf{c}_i$ and $\mathbf{c}_j$ to the contact point, respectively. Let $\mathbf{n}$ be the

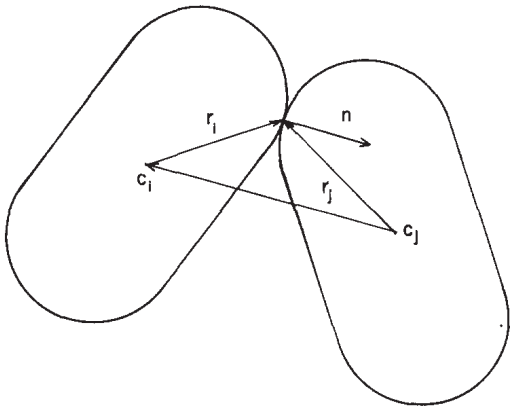

Figure 1: Two spherocylinders i and j in contact with each other. $\mathbf{r}_i$ and $\mathbf{r}_j$ are the vectors from the center $\mathbf{c}_i$ and $\mathbf{c}_j$ to the contact point, respectively. $\mathbf{n}$ is the unit outward normal vector to the surface of spherocylinder i at the contact point.

outward unit normal vector to the surface of the spherocylinder i at the contact point. After collision, the translational velocity and the angular momentum are given by [21]

$$\begin{aligned}
\mathbf{p}_i' &= \mathbf{p}_i + \Delta\mathbf{p}_{ji}, \\
\mathbf{p}_j' &= \mathbf{p}_j - \Delta\mathbf{p}_{ji}, \\
\boldsymbol{\omega}_i' &= \boldsymbol{\omega}_i + \mathbf{r}_i \times \Delta\mathbf{p}_{ji}/I, \\
\boldsymbol{\omega}_j' &= \boldsymbol{\omega}_j - \mathbf{r}_j \times \Delta\mathbf{p}_{ji}/I,
\end{aligned} \tag{2.4}$$

where $\Delta\mathbf{p}_{ji}$ is the collision impulse given by

$$\Delta\mathbf{p}_{ji} = \frac{\langle -\mathbf{g}_{ij}, \mathbf{n}\rangle \mathbf{n}}{1 + (|\mathbf{r}_i \times \mathbf{n}|^2 + |\mathbf{r}_j \times \mathbf{n}|^2)/2I}, \tag{2.5}$$

where $\mathbf{g}_{ij} = \mathbf{p}_i - \mathbf{p}_j + \boldsymbol{\omega}_i \times \mathbf{r}_i - \boldsymbol{\omega}_j \times \mathbf{r}_j$ is the velocity of particle i relative to particle j and $\langle \cdot, \cdot \rangle$ denotes the inner product between two vectors.

The internal pressure of the system can be computed using the following formula [22]:

$$P_{\text{int}} = \frac{1}{3V}\left[\sum_{i=1}^{N} \mathbf{p}_i^2 + \sum_{i=1}^{N} \langle \mathbf{F}_i, \mathbf{c}_i \rangle\right], \tag{2.6}$$

where V is the total volume of the system, and $\mathbf{F}_i$ is the total force exerted on the particle i

$$\mathbf{F}_i = \sum_{k=1}^{N} \mathbf{F}_{ki}, \tag{2.7}$$

where $\mathbf{F}_{ki}$ is the force exerted by the particle k on the particle i and $\mathbf{F}_{ii}=0$. Hence, we can rewrite the second term in Eq. (2.6) as

$$\begin{aligned}\sum_{i=1}^{N}\langle\mathbf{F}_i,\mathbf{c}_i\rangle &= \sum_{i=1}^{N}\sum_{k=1}^{N}\langle\mathbf{F}_{ki},\mathbf{c}_i\rangle \\ &= \sum_{i=2}^{N}\sum_{k=1}^{i-1}\langle\mathbf{F}_{ki},\mathbf{c}_i\rangle + \sum_{i=1}^{N-1}\sum_{k=i+1}^{N}\langle\mathbf{F}_{ki},\mathbf{c}_i\rangle \\ &= \sum_{i=2}^{N}\sum_{k=1}^{i-1}\langle\mathbf{F}_{ki},\mathbf{c}_i\rangle + \sum_{k=1}^{N-1}\sum_{i=k+1}^{N}\langle-\mathbf{F}_{ki},\mathbf{c}_k\rangle \\ &= \sum_{i=2}^{N}\sum_{k=1}^{i-1}\langle\mathbf{F}_{ki},(\mathbf{c}_i-\mathbf{c}_k)\rangle, \end{aligned} \tag{2.8}$$

where we have used the fact that $\mathbf{F}_{ki}=-\mathbf{F}_{ik}$. Therefore the internal pressure P_{int} can be rewritten as

$$P_{\text{int}}=\frac{1}{3V}\left[\sum_{i=1}^{N}\mathbf{p}_i^2+\sum_{i=2}^{N}\sum_{k=1}^{i-1}\langle\mathbf{F}_{ki},(\mathbf{c}_i-\mathbf{c}_k)\rangle\right]. \tag{2.9}$$

For the system considered here, the forces $\mathbf{F}_{ki}$ are singular as the inter particle potential is infinite when two particles collide and zero otherwise. In the computation, we approximate the forces by the change of momentum per unit time given by [16]

$$\mathbf{F}_{ki}(t)\approx\frac{1}{\tau}\sum\Delta\mathbf{p}_{ki}, \tag{2.10}$$

where the summation is taken over all collisions between particle k and i within the time window $[t-\tau,t]$, and $\Delta\mathbf{p}_{ki}$ is the collision impulse given in Eq. (2.5). If no collision occurs in the time window $[t-\tau,t]$, we set $\mathbf{F}_{ki}(t)=0$.

We study the system using MD simulation in the isothermal-isobaric (NPT) ensemble, in which the pressure and temperature of the system are maintained at prescribed values. The MD algorithm is based on the one in Ref. [23] which was originally proposed for systems of spherical particles. In this work, the scheme is modified to adapt to the hard spherocylinder system. We use the Langevin dynamics to control the temperature. To control the pressure, the volume of the system evolves according to

$$\begin{aligned}\dot{V} &= \frac{3p_b}{W}V, \\ \dot{p_b} &= 3V(P_{\text{int}}-P),\end{aligned} \tag{2.11}$$

where p_b is the barostat moment, W is the barostat mass and P is the external pressure. At each MD time step, we check whether collision occurs between particles. Two spherocylinders collide when they overlap and their relative motion is towards each other,

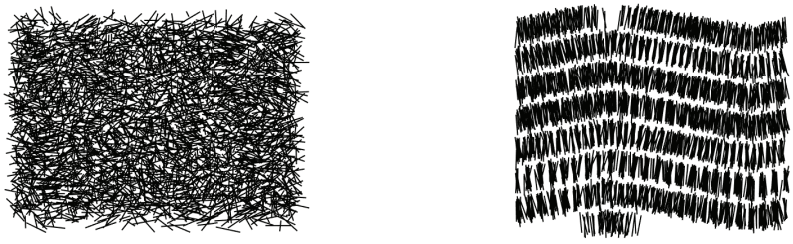

Figure 2: The isotropic phase (left) and the nematic phase (right) of the spherocylinder system obtained from the MD simulation.

namely: (1) $r < D$ and (2) $\langle \mathbf{g}_{ij}, \mathbf{n} \rangle > 0$, where r is the distance between the two line segments on the central axes of the cylinder part of the two spherocylinders, and $D = 2R$ is the diameter of the cylinder.

We use $N = 3087$ spherocylinders with an aspect ratio $h/D = 2$ in a cubic periodic box. We use D and $k_B T$ as the unit of length and the unit of energy, respectively. The internal pressure P_{int} is computed by Eq. (2.10) with observation time $\tau = 1$. The external pressure is fixed at $P = 6.5$. At this pressure, the system exhibits two metastable phases: the isotropic phase and the nematic phase as shown in Fig. 2. This is consistent with the phase diagram in Ref. [18]. The transition from one phase to another never occurs on the time scale of our simulation. In the simulation, the volume is updated according to Eq. (2.11) to control the internal pressure. The difference of the volume between the isotropic phase and the nematic phase is about 16%. Thus, the volume V can be identified as a coarse-grained variable to distinguish the two metastable phases. In the next section, we will introduce another coarse-grained variable, called the order parameter, to characterize the two phases.

3 Isotropic-nematic phase transition

3.1 Collective variables and MFEP

The volume of the system V and the order parameter S are used as the collective variables (CVs) to study the isotropic-nematic phase transition. The order parameter measures the ordering of the spherocylinders along a common direction. To define the order parameter, we consider the following tensor Q

$$Q_{\alpha,\beta} = \frac{1}{N}\left(\sum_{i=1}^{N} \frac{3}{2} u_{i\alpha} u_{i\beta}\right) - \frac{1}{2}\delta_{\alpha\beta}, \quad \alpha,\beta = x,y,z, \tag{3.1}$$

where the sum is taken over all spherocylinders in the system, u_{ix}, u_{iy}, u_{iz} are the three components of the symmetry axis $\mathbf{u}$ of the spherocylinder i, and $\delta_{\alpha\beta} = 1$ if $\alpha = \beta$ and 0 otherwise. The order parameter S is given by the largest eigenvalue of Q [13]. The

corresponding eigenvector, denoted by $\mathbf{v}$ with $\|\mathbf{v}\|=1$, is called the nematic director. For the two phases shown in Fig. 2, the order parameter is $S\approx 0$ for the isotropic phase and $S\approx 1$ for the nematic phase.

For ease of presentation, we define the vector $\mathbf{r}=(\mathbf{c},\mathbf{u},V)$ which consists of the position and orientation vectors of all the spherocylinders and the volume of the system. Furthermore, we denote the two collective variables by $\boldsymbol{\theta}=(\theta_1,\theta_2)$, where $\theta_1(\mathbf{r})=V$ and $\theta_2(\mathbf{r})=S$. The free energy in the CVs space is given by

$$F(\mathbf{z})=-k_BT\ln\left(Z^{-1}\int e^{-H(\mathbf{r})/k_BT}\delta(z_1-\theta_1(\mathbf{r}))\delta(z_2-\theta_2(\mathbf{r}))d\mathbf{r}\right), \tag{3.2}$$

where $\mathbf{z}=(z_1,z_2)$, $H(\mathbf{r})=\sum_{i\neq j}U(d_{ij})+PV$ with d_{ij} being the surface-to-surface distance between particles i and j, and $\delta(\cdot)$ is the Dirac delta function. The minimum free energy path (MFEP), which is denoted by $\mathbf{z}(\alpha)$ with $\alpha\in[0,1]$ being the parameterization of the path, is defined as the curve in the CVs space which connects two local minima of the free energy $F(\mathbf{z})$ and satisfies the following condition [10]:

$$\mathbf{z}'(\alpha)\parallel M(\mathbf{z}(\alpha))\nabla_{\mathbf{z}}F(\mathbf{z}(\alpha)),\quad \alpha\in[0,1], \tag{3.3}$$

where $M(\mathbf{z})$ is the matrix given by

$$M_{ij}(\mathbf{z})=\left\langle\nabla_{\mathbf{r}}\theta_i\cdot\nabla_{\mathbf{r}}\theta_j\right\rangle_{\boldsymbol{\theta}=\mathbf{z}},\quad i,j=1,2, \tag{3.4}$$

where $\langle\cdot\rangle_{\boldsymbol{\theta}=\mathbf{z}}$ denotes the ensemble average with the CVs constrained at the target value $\mathbf{z}$. The matrix M and the mean force $-\nabla_{\mathbf{z}}F$ can be computed using restrained MD simulations [10]. Specifically, to constrain the volume V at z_1, an additional force corresponding to the potential $\frac{\kappa}{2}(V-z_1)^2$ is added to Eq. (2.11):

$$\dot{p}_b=3V(P_{\text{int}}-P)-\kappa(V-z_1). \tag{3.5}$$

Similarly, we introduce the harmonic potential $\frac{\kappa}{2}(S-z_2)^2$ to constrain the order parameter S at z_2. The angular momentum of each spherocylinder evolves according to

$$\dot{\boldsymbol{\omega}}_k=-(\mathbf{u}_k\times\kappa(S(\mathbf{r})-z_2)\nabla_{\mathbf{u}_k}S), \tag{3.6}$$

where $\mathbf{u}_k=(u_x,u_y,u_z)$ is the symmetry axis of particle k and $\nabla_{\mathbf{u}_k}S=(\frac{\partial S}{\partial u_x},\frac{\partial S}{\partial u_y},\frac{\partial S}{\partial u_z})$. For ease of notation, we have neglected the subscript k in the components u_x, u_y and u_z. The matrix M and the mean force $-\nabla_{\mathbf{z}}F$ can be computed by time-averaging $\nabla_{\mathbf{r}}\theta_i\cdot\nabla_{\mathbf{r}}\theta_j$ and $-\kappa(z_j-\theta_j(\mathbf{r}))$ following the trajectory of the restrained MD, respectively [10].

The vector $\nabla_{\mathbf{u}_k}S$ in Eq. (3.6) is computed as follows. Let $\mathbf{v}$ be the unit eigenvector corresponding to S. Then we have $S=\mathbf{v}^TQ\mathbf{v}$. The differential of S is given by $dS=(d\mathbf{v})^TQ\mathbf{v}+\mathbf{v}^TdQ\mathbf{v}+\mathbf{v}^TQd\mathbf{v}$. Since $\|\mathbf{v}\|=1$, we have $d\|\mathbf{v}\|^2=2(d\mathbf{v})^T\mathbf{v}=2\mathbf{v}^Td\mathbf{v}=0$. Therefore $dS=\mathbf{v}^TdQ\mathbf{v}$. So we can compute $\nabla_{\mathbf{u}_k}S$ using

$$\frac{\partial S}{\partial u_i}=\mathbf{v}^T\frac{\partial Q}{\partial u_i}\mathbf{v},\quad i=x,\,y,\,z, \tag{3.7}$$

where

$$\frac{\partial Q}{\partial u_x}=\frac{1}{N}\begin{bmatrix}3u_x & \frac{3}{2}u_y & \frac{3}{2}u_z\\ \frac{3}{2}u_y & 0 & 0\\ \frac{3}{2}u_z & 0 & 0\end{bmatrix}, \tag{3.8}$$

$$\frac{\partial Q}{\partial u_y}=\frac{1}{N}\begin{bmatrix}0 & \frac{3}{2}u_x & 0\\ \frac{3}{2}u_x & 3u_y & \frac{3}{2}u_z\\ 0 & \frac{3}{2}u_z & 0\end{bmatrix}, \tag{3.9}$$

$$\frac{\partial Q}{\partial u_z}=\frac{1}{N}\begin{bmatrix}0 & 0 & \frac{3}{2}u_x\\ 0 & 0 & \frac{3}{2}u_y\\ \frac{3}{2}u_x & \frac{3}{2}u_x & 3u_z\end{bmatrix}. \tag{3.10}$$

3.2 The string method

We use the on-the-fly string method in collective variables [10, 11] to compute the MFEP connecting the two local minima on the free energy landscape. The two local minima, which correspond to the isotropic phase and the nematic phase respectively, are shown in Fig. 3. In the figure, we have rescaled the variable z_1 by the factor 1650 which approximates the difference of the volume between the two phases. In the presentation below, we will use this rescaled variable. With a slight abuse of notation, we still denote it using z_1.

The initial string is constructed using the linear interpolation between the two local minima in the CVs space. In the computation, the string is discretized into $N=35$ images $\{\mathbf{z}_1,\cdots,\mathbf{z}_N\}$ by equal arc length. For each image $\mathbf{z}_k$, we assign an atomistic replica $\mathbf{r}_k$. The replica $\mathbf{r}_k$ is constrained at the target value $\mathbf{z}_k$ of the CVs. The discretized string and the corresponding atomistic replicas are evolved using the time step Δt during the simulation. Denote by $\mathbf{z}_k^n$ and $\mathbf{r}_k^n$ the k-th image and the corresponding atomistic replica at time $t_n=n\Delta t$, respectively. At each time step, the discrete images and the corresponding replicas are updated following the two-step procedure:

1. Evolve each image $\mathbf{z}_k^n$ and the corresponding replica $\mathbf{r}_k^n$, where $k=1,\cdots,N$, concurrently by one time step Δt:

   - Update the atomistic replica $\mathbf{r}_k^n$ by running the restrained MD as discussed in the previous section by one time step with the collective variables $\boldsymbol{\theta}(\mathbf{r})$ constrained at $\mathbf{z}_k^n$. The new configuration of the replica is denoted by $\mathbf{r}_k^{n+1}$.
   - Estimate the matrix M and the mean force using $\mathbf{r}_k^{n+1}$:

   $$M_{ij}\approx\nabla_{\mathbf{r}}\theta_i(\mathbf{r}_k^{n+1})\cdot\nabla_{\mathbf{r}}\theta_j(\mathbf{r}_k^{n+1}),\quad i,j=1,2, \tag{3.11}$$

   $$\nabla_{\mathbf{z}}F\approx\kappa(\mathbf{z}_k^n-\boldsymbol{\theta}(\mathbf{r}_k^{n+1})), \tag{3.12}$$

   then evolve the image $\mathbf{z}_k^n$ using the forward Euler scheme by one time step

   $$\mathbf{z}_k^*=\mathbf{z}_k^n-\frac{\Delta t}{\gamma}M\nabla_{\mathbf{z}}F. \tag{3.13}$$

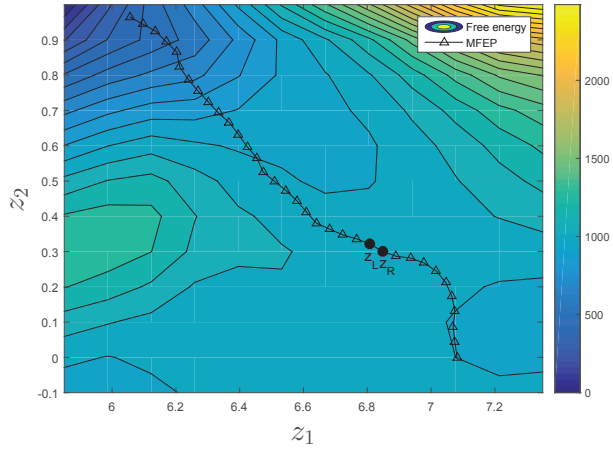

Figure 3: The MFEP connecting the nematic phase (top left) and the isotropic phase (bottom right). The variable z_1 has been rescaled by the difference of the volume between the isotropic and nematic phases. Along the MFEP, the free energy attains the maximum between the two images marked by filled circles. The background shows the contour plot of the free energy constructed using radial basis functions.

The parameter γ is chosen large enough to slow down the dynamics of the string, so that the atomistic replica has enough time to equilibrate at the current value of the CVs.

2. To ensure a uniform distribution of the images along the string, the images $\mathbf{z}_k^*$, where $k=1,\cdots,N$, are redistributed using the linear interpolation. The new images are denoted by $\mathbf{z}_k^{n+1}$. For details of the interpolation algorithm, we refer to the original paper on the string method [6–8].

The above two steps are repeated until the string reaches the steady state. At the steady state, the string locates the MFEP which gives the most probable pathway for the isotropic-nematic phase transition.

3.3 Numerical results

In the computation, the parameters are taken as $\kappa=10^5$ and $\gamma=10^3$, $\Delta t=0.001$. Fig. 3 shows the contour plot of the free energy $F(z_1,z_2)$ and the MFEP. The free energy was computed using the single-sweep method [24]. The algorithm of the single-sweep method is reviewed in Appendix B. The MFEP connects the nematic phase (top left) and the isotropic phase (bottom right). The deviation of the end points of the string from the local minima is due to the small magnitude of the mean force near the minima, and the error in the construction of the free energy using a finite number of radial basis functions. We notice that the free energy was not used in the calculation of the MFEP. The MFEP was computed using the mean force obtained from the atomistic configurations. We also notice that the MFEP does not follow the MEP of the free energy due to the tensor M

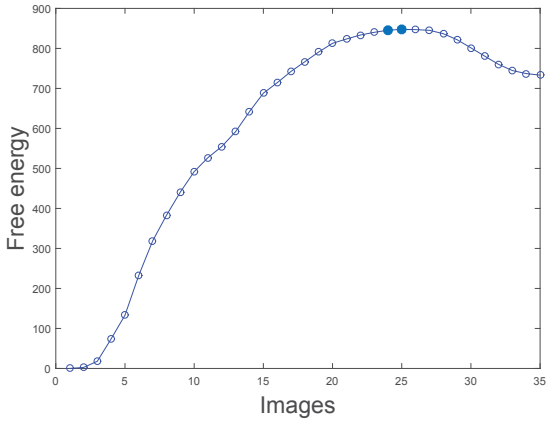

Figure 4: The free energy along the MFEP. The maximum of the free energy occurs between the two images marked by filled circles.

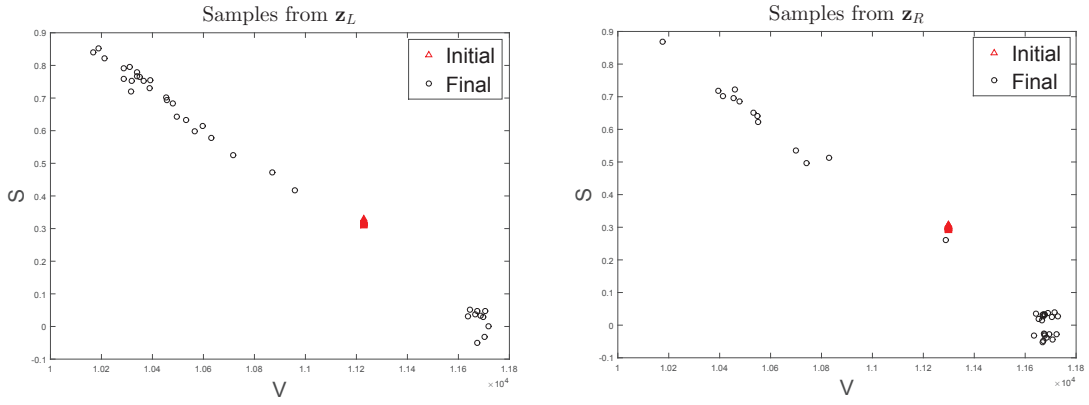

Figure 5: The volume V and order parameter S of the 35 atomistic configurations sampled from $\mathbf{z}_L$ (left) and $\mathbf{z}_R$ (right) respectively after a certain number of steps of relaxation. The initial position of the samples are marked by triangles ($\triangle$). About 71.4% of the samples from $\mathbf{z}_L$ (left) relaxed towards the nematic phase ($S\approx 1$), while about 65.7% of the samples from $\mathbf{z}_R$ (right) relaxed towards the isotropic phase ($S=0$).

involved in the definition of the MFEP in Eq. (3.3). The free energy along the MFEP is shown in Fig. 4. The maximum of the free energy along the MFEP occurs between the two images marked by filled circles in Fig. 3. These two images are denoted by $\mathbf{z}_L$ and $\mathbf{z}_R$, respectively.

The transition state lies in between the images $\mathbf{z}_L$ and $\mathbf{z}_R$. To verify this, we sampled 35 atomistic configurations from $\mathbf{z}_L$ and $\mathbf{z}_R$, respectively. These samples were then released and they relaxed to one of the two metastable phases. In Fig. 5, we plot the position of these samples in the CVs space after a certain number of time steps of relaxation. It shows that most of the samples from $\mathbf{z}_L$ (71.4%) evolved to the nematic phase, while most of the samples from $\mathbf{z}_R$ (65.7%) evolved to the isotropic phase. This confirms that

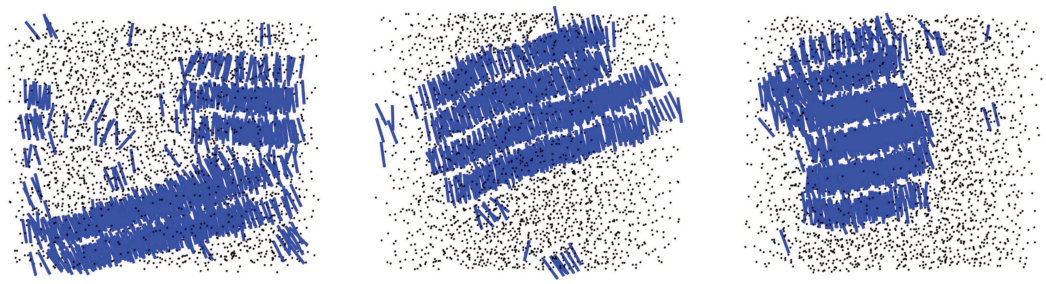

Figure 6: Typical atomistic configurations sampled from $\mathbf{z}_R$. Particles in the isotropic phase and in the nematic phase are represented by dots ($\cdot$) and rods ($|$), respectively. A particle is classified as being in the nematic phase if its local order parameter is larger than 0.4.

the transition state, at which the system has equal probability to evolve to each of the two metastable phases, lies in between the images $\mathbf{z}_L$ and $\mathbf{z}_R$.

Next, we examine the local structures of those atomistic configurations sampled from $\mathbf{z}_R$. The local structure of the spherocylinder system can be characterized by the local order parameter given by [3]

$$S_{loc}(i)=\frac{1}{n_i}\sum_{j=1}^{n_i}\left(\frac{3}{2}|\mathbf{u}_i\cdot\mathbf{u}_j|^2-\frac{1}{2}\right), \tag{3.14}$$

where n_i is the number of particles in the neighborhood of particle i. The particle is considered to be in the neighborhood of the particle i if their face-to-face distance is less than $1.5D$. This local order parameter describes the nematic ordering of a particle with respect to its neighboring particles. The particle i is classified as in the nematic phase if the local order parameter $S_{loc}(i)>K$. We use $K=0.4$ following Ref. [3]. With this criterion, we can identify the nematic cluster(s) formed during the isotropic-nematic phase transition.

Different atomistic structures are observed in the samples from $\mathbf{z}_R$. Fig. 6 shows three representative structures of the nematic cluster. Multilayer structures are observed in all the three samples. There are two separated clusters in the first sample and only one cluster in the other two samples. Moreover, we found that the stability of the nematic cluster depends on its size, which can be seen from Fig. 7. The figure shows the order parameter S of the final state after free relaxation versus the number of nematic particles in the initial state. It can be seen that the samples with more nematic particles are more likely to evolve to the nematic phase under free relaxation.

4 Conclusions

In this work, we studied the isotropic-nematic phase transition of liquid crystals using an atomistic model consisting of spherocylinders. We employed the order parameter and the volume of the particle system as the collective variables and computed the MFEP

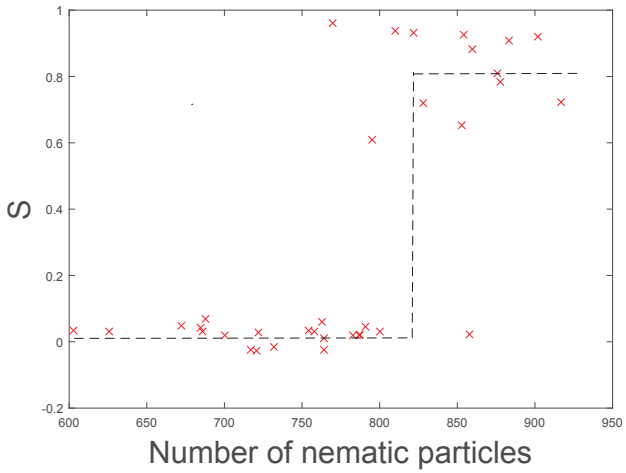

Figure 7: The order parameter S of the samples from $\mathbf{z}_R$ after relaxation versus the number of nematic particles in the initial configuration of the samples. The dashed line is a fit of the pattern of the points.

in the collective variable space using the string method. The transition state was identified along the MFEP. It was observed that the isotropic-nematic phase transition occurs via nucleation of nematic clusters, which exhibit multilayer structures near the transition state. The nematic nucleus with more nematic-like particles is more likely to evolve towards the nematic phase.

In this study, only the global order parameter and the volume of the system are used as collective variables. This reduces the complexity of the computation. More detailed descriptions, for example, by including the local order parameter in the CVs space, will be investigated in our future work. This will help better quantify the structures of the transition state at the microscopic level.

Acknowledgments

The work was partially supported by Singapore MOE AcRF Tier-1 grant R-146-000-216-112 and Singapore MOE AcRF Tier-2 grant R-146-000-232-112.

Appendices

A Mass momentum of inertia

The mass momentum of inertia of the spherocylinder, shown in Fig. 8, with respect to the x axis is the sum of the corresponding moments of the cylinder and of the two hemispheres:

$$I_x = I_x^c + 2I_x^s. \tag{A.1}$$

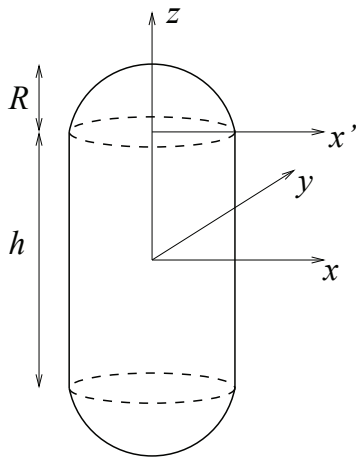

Figure 8: Schematics of the spherocylinder.

The moment of the cylinder around the x axis is given by

$$I_x^c = \int_{\Omega_c} (z^2+y^2)\rho dV = \frac{1}{12}\pi\rho R^2 h^3 + \frac{1}{4}\pi\rho R^4 h, \tag{A.2}$$

where ρ is the (constant) mass density of the spherocylinder, and the volume integral is over the whole cylinder. Using the parallel axis theorem, the moment of inertia of a hemisphere around the x axis is given by

$$I_x^s = I_{x'}^s - m z_{CM}^2 + m\left(\frac{1}{2}h + z_{CM}\right)^2, \tag{A.3}$$

where $I_{x'}^s$ is the moment of the hemisphere around the axis through the center of the sphere as shown in Fig. 8, $m = \frac{2}{3}\pi\rho R^3$ is the mass of the hemisphere, and $z_{CM} = \frac{3}{8}R$ is distance of the center of mass of the hemisphere to the center of the sphere. The moment of the hemisphere $I_{x'}^s$ is simply half of the moment of the whole sphere

$$I_{x'}^s = \frac{1}{2}\cdot\frac{8}{15}\pi\rho R^5 = \frac{4}{15}\pi\rho R^5. \tag{A.4}$$

Inserting the above results in Eq. (A.3) yields

$$I_x^s = \pi\rho R^3\left(\frac{4}{15}R^2 + \frac{1}{6}h^2 + \frac{1}{4}Rh\right). \tag{A.5}$$

The summation of I_x^c in (A.2) and twice of I_x^s in (A.5) yields the formula for the moment of the spherocylinder given in (2.1).

B Free energy calculation

To construct the free energy surface, we use the single-sweep method proposed in Ref. [24]. First, we use the temperature accelerated molecular dynamics to explore the configuration space of the particle system, and generate K centers $\mathbf{z}_1,\cdots,\mathbf{z}_K$ in the CVs space. Then the mean force f_k is calculated at each center using a time averaging approach [10]. These forces are used to construct the free energy surface using a set of radial basis functions (RBFs).

We write the free energy $F(\mathbf{z})$ as a linear combination of RBFs:

$$F(\mathbf{z})=\sum_{k=1}^{K}a_k\phi_\sigma(|\mathbf{z}-\mathbf{z}_k|), \tag{B.1}$$

where $\phi_\sigma(r)=\exp(-r^2/2\sigma^2)$ is a Gaussian kernel with width σ. In [24], the coefficients a_k and the width σ are determined via the minimization of the error function

$$E(a,\sigma)=\sum_{k=1}^{K}|f_k+\nabla_{\mathbf{z}}F(\mathbf{z}_k)|^2, \tag{B.2}$$

where $a=(a_1,a_2,\cdots,a_K)$. This error function measures the absolute error in the approximation of the mean force. For the spherocylinder system considered in this work, the magnitude of the mean force is significantly larger at some centers than others, so the terms in the summation in Eq. (B.2) are at different scales. Hence, it makes more sense to minimize the relative error instead,

$$\tilde{E}(a,\sigma)=\sum_{k=1}^{K}\frac{|f_k+\nabla_{\mathbf{z}}F(\mathbf{z}_k)|^2}{|f_k|^2}. \tag{B.3}$$

For a fixed value of σ, the minimization of the error function $\tilde{E}(a,\sigma)$ over the coefficients can be done by solving a system of linear equations for a_k. This calculation is carried out for a range of values of σ to find the optimal choice for the width of the RBFs.

The free energy for the spherocylinder system is shown in Fig. 3. The free energy was constructed using $K=47$ centers, which were generated by the temperature accelerated molecular dynamics with the pairwise distance $d>0.165$.

References

[1] A. Kuijk, D. V. Byelov, A. V. Petukhov, A. van Blaaderen, A. Imhof, Phase behavior of colloidal silica rods, Faraday Discuss., 159, 181-199 (2012).
[2] H. Maeda, Y. Maeda, Liquid crystal formation in suspensions of hard rodlike colloidal particles: Direct observation of particle arrangement and self-ordering behavior, Phys. Rev. Lett., 90, 018303 (2003).
[3] A. Cuetos, R. van Roij, M. Dijkstra, Isotropic-to-nematic nucleation in suspensions of colloidal rods, Soft Matter, 4, 757-767 (2008).

[4] A. Patti, M. Dijkstra, Do multilayer crystals nucleate in suspensions of colloidal rods? Phys. Rev. Lett., 102, 128301 (2009).
[5] T. Schilling, D. Frenkel, Self-poisoning of crystal nuclei in hard-rod liquids, Phys. Rev. Lett., 92, 085505 (2004).
[6] W. E, W. Ren, E. Vanden-Eijnden, String method for study of rare events, Phys. Rev. B, 66, 052301 (2002).
[7] W. Ren, High order numerical scheme in the string method for finding minimum energy paths and saddle points, Commun. Math. Sci., 1, 377 (2003).
[8] W. E, W. Ren, E. Vanden-Eijnden, Simplified and improved string method for computing the minimum energy paths in barrier-crossing events, J. Chem. Phys., 126, 164103 (2007).
[9] W. Ren, E. Vanden-Eijnden, A climbing string method for saddle point search, J. Chem. Phys., 138, 134105 (2013).
[10] L. Maragliano, A. Fischer, E. Vanden-Eijnden, G. Ciccoti, String method in collective variables: Minimum free energy paths and isocommittor surfaces, J. Chem. Phys., 125, 024106 (2006).
[11] L. Maragliano, E. Vanden-Eijnden, On-the-fly string method for minimum free energy paths calculation, Chem. Phys. Lett., 446, 182-190 (2007).
[12] L. Onsager, The effects of shape on the interaction of colloidal particles, Ann. NY Acad. Sci., 51, 627-659 (1949).
[13] P. G. De Gennes, The Physics of Liquid Crystals, Clarendon Press Oxford, 1974.
[14] G. A. Few, M. Rigby, Equation of state for systems of hard non-spherical molecules, Chem. Phys. Lett., 20, 433-435 (1973).
[15] J. Vieillard-Baron, The equation of state of a system of hard spherocylinders, Molecular Physics, 28, 809-818 (1974).
[16] D. W. Rebertus, K. M. Sando, Molecular dynamics simulation of a fluid of hard spherocylinders, J. Chem. Phys., 67, 2585 (1977).
[17] J. A. C. Veerman, D. Frenkel, Phase diagram of a system of hard spherocylinders by computer simulation, Phys. Rev. A, 41, 3237 (1990).
[18] P. Bolhuis, D. Frenkel, Tracing the phase boundaries of hard spherocylinders, J. Chem. Phys., 106, 666-687 (1997).
[19] T. Q. Yu, P. Y. Chen, M. Chen, A. Samanta, E. Vanden-Eijnden, M. Tuckerman, Order-parameter-aided temperature-accelerated sampling for exploration of crystal polymorphism and solid-liquid phase transitions, J. Chem. Phys., 140, 214109 (2014).
[20] L. Zhang, W. Ren, A. Samanta, Q. Du, Recent developments in computational modeling of nucleation in phase transformations, npj Computational Materials, 2, 16003 (2016).
[21] M. P. Allen, D. Frenkel, J. Talbot, Molecular dynamics simulation using hard particles, Comp. Phys. Rep., 9, 301-353 (1989).
[22] S. H. Lee, H. S. Kim, H. Pak, A molecular dynamics simulation study on nematic-isotropic phase transition of rod-like molecules in NPT ensemble, J. Chem. Phys., 97, 6933-6941 (1992).
[23] G. Bussi, T. Zykova-Timan, M. Parrinello, Isothermal-isobaric molecular dynamics using stochastic velocity rescaling, J. Chem. Phys., 130, 074101 (2009).
[24] L. Maragliano, E. Vanden-Eijnden, Single-sweep methods for free energy calculations, J. Chem. Phys., 128, 184110 (2008).